Fizika Nizkikh Temperatur, 2002, v. 28, No. 7, p. 691–708

Elementary excitations in solid oxygen

(Review Article)

Yu. A. Freiman

B. Verkin Institute for Low Temperature Physics and Engineering of the National Academy of Sciences of Ukraine, 47 Lenin Ave., Kharkov 61103, Ukraine
E-mail: freiman@ilt.kharkov.ua

H. J. Jodl

Fachbereich Physik, Universität Kaiserslautern, Erwin Schrödinger Strasse, D 67663 Kaiserslautern, Germany
E-mail: jodl@physik.uni-kl.de
LENS, European Laboratory for Non Linear Spectroscopy, Largo E. Fermi 2, I-50125 Firenze, Italy
E-mail: jodl@lens.unifi.it

Received May 13, 2002

Theoretical results on lattice excitations in solid oxygen at equilibrium vapor pressure are reviewed with the emphasis on the behavior of phonons, librons and magnons in the orientationally and magnetically ordered α-phase. Results on magnetooptics of solid oxygen and their impact on advance of magnetic studies of solid oxygen are briefly reviewed. Some results under discussion are new: among these are theoretical results on the magnon heat capacity, the analysis of the behavior of librons at the α–β transition, anisotropy of the spectrum of magnons.

PACS: 75.50.Ee, 75.50.Xx, **75.40.–s**, 78.20.Ls, **78.30.–j**, **63.20.–e**

Contents

1. Introduction. Solid oxygen, a unique combination of a molecular cryocrystal and a magnet

Solid oxygen belongs to a small group of atomic (He, Ne, Ar, Kr, Xe) or simple molecular solids (H_2, N_2, O_2, F_2, CO, CO_2, N_2O, CH_4), which are often lumped together as solidified gases or cryocrystals.

The oxygen molecule owing to unique combination of the molecular parameters forms the substance which in all phases, solid, liquid or gaseous, is a physical object of considerable fundamental interest.

In the ground electronic state the oxygen molecule possesses nonzero electronic spin $S=1$, which makes the O_2 molecule a magnetic system. As a result, solid oxygen combines properties of a molecular crystal and that of a magnet.

The low-temperature phase of solid oxygen is the only electron-spin antiferromagnetic insulator consisting of a single element. Why the combination of a simple molecular crystal and a magnet is so interesting? The answer is the following: the binding

energy in molecular cryocrystals is determined by weak Van der Waals forces and, unlike conventional magnets, the magnetic interaction is a significant part of the total lattice energy. Namely, the binding energy in the case of solid oxygen is of the order 1000 K and the magnetic energy is of the order of 100 K, that is, makes up around 10% of the binding energy. In the case of conventional magnets, the magnetic energy is of the same order, but the binding energy is an order of magnitude higher, that is the magnetic energy is at most about 1% of the lattice energy. Therefore the magnetic and lattice properties in solid oxygen are very closely related which manifests itself in numerous anomalies of virtually all its properties — thermal, magnetic, acoustic, optical, etc.

A start of studies of solid oxygen has been made at the very beginning of the twentieth century. The modern state of art is a result of combined continuous efforts of a large number of cryogenic laboratories throughout the world. At the present time solid oxygen is a playground for the most sophisticated modern solid-state experimental methods including studies in diamond anvil cells (DAC) and high magnetic fields in combination with Raman, infrared (FIR, FTIR), synchrotron x-ray, and Brillouin and other optical technics.

Under equilibrium vapor pressure oxygen exists in three crystallographic modifications [1].

Neutron diffraction [2–5] and x-ray studies [1,6,7] showed that the low-temperature α phase of oxygen is orientationally and magnetically ordered and has a monoclinic base-centered structure of symmetry $C2/m$. It was established that α-O_2 has the simplest orientational structure, in which the molecular axes are collinear and perpendicular to the close-packed (001) layers (Fig. 1).

The structure of the intermediate β phase of solid oxygen was established by Hörl in the electron-diffraction study [8] and confirmed in the neutron-diffraction [2–5], and x-ray studies [1,7]. It was shown that β-O_2 has a rhombohedral lattice of symmetry $R\bar{3}m$ with the same simplest orientational structure as α-O_2 (Fig. 2,*a*). This lattice can be seen as a distorted fcc structure obtained by packing not spherical but dumb-bell shaped molecules oriented along one of the spatial diagonals of the cube. The primitive rhombohedral cell is found to be stretched in the direction <111> singled out by the molecular axes. The angle of the rhombohedron is found to be about 45° instead of 60° for fcc lattice.

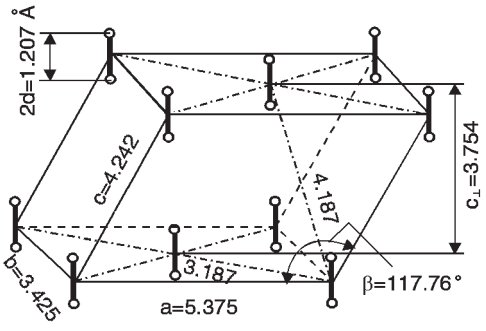

Fig. 1. Structure of α-O_2.

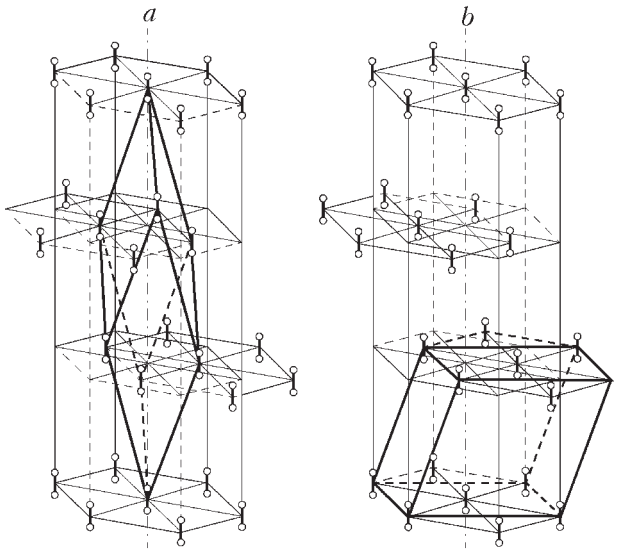

Fig. 2. Structure of β-O_2 in rhombohedral and hexagonal axes (*a*). The structure of β-O_2 can be represented as a monoclinic cell isostructural to α-O_2 (*b*).

The structures of the two low-temperature phases are similar, and formally, a monoclinic cell can be singled out in β-O_2 as well (Fig. 2,*b*).

As was shown in a single-crystal x-ray study by Jordan et al. [9], γ-O_2 has an eight-molecule cubic cell with an orientationally disordered structure of space group $Pm3n$ (Fig. 3). Molecules in the cell are located in two nonequivalent states. Two of the eight molecules («spheres») have a spherically symmetric distribution of electron density while the remaining six molecules («discs») have electron

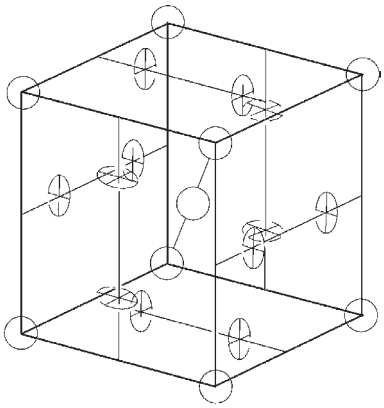

Fig. 3. Structure of γ-O_2.

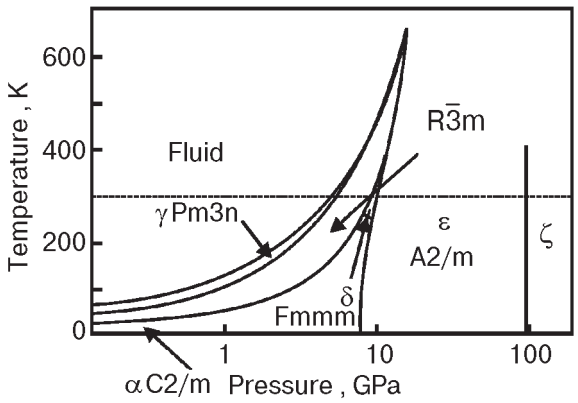

Fig. 4. Phase diagram of solid oxygen.

density distribution in the form of an oblate spheroid. The disc-shaped molecules form chains extending in three <100> directions.

At the present time the existence of six solid-state phases is established unambigously [10]. In addition to the α, β, and γ phases existing under equilibrium vapor pressure three high pressure stable phases exist in the studied domain of pressures and temperatures. They are the δ («orange») stable at room temperature between 9.6 and 10 GPa, ϵ («red») (10–96 GPa) and ς (metallic) (above 96 GPa) phases. The resulting $P-T$ phase diagram which reflects the phase boundaries of these six phases is given in Fig. 4.

2. Characteristic features of elementary excitation spectra in solid oxygen

Compared with a conventional magnet, the problem of the elementary excitation spectrum in solid oxygen presents a considerable challenge both to the experimenters and theoriticians. In the case of α-O_2 we are dealing with three systems of coupling quasiparticles — phonons, librons, and magnons. Though β-O_2 has the simplest orientational structure among the molecular cryocrystals, the presence of the strong short-range magnetic order makes the β phase quite a cumbersome problem. Very specific case is the orientationally and magnetically disordered γ phase.

First calculations of the lattice dynamics of solid oxygen were carried out in the 1970s [1,7,11,12]. Though no account has been taken in these calculations of the magnetic nature of solid oxygen, they represent a necessary and rather informative step in the development of the theory. They provided a test, in the first approximation, of various potentials, enabled the identification in Raman and IR spectra, and gave an estimate of the effect of anharmonicity.

Important estimates concerning translational and librational vibrations follow from simple mean-field considerations [13,14]. Translationally the molecules in α-O_2 vibrate as three-dimensional, nearly harmonic oscillators. Two of the fundamental frequencies that correspond with the vibrations in the *ab* plane are near equal, the third fundamental frequency for the vibrations in the $c_\perp$ direction is about 50% larger. The potential is markedly stiffer in the $c_\perp$ direction. This is confirmed by the smaller root-mean-square (rms) amplitude of vibrations in this direction (Table). As can be seen from this Table, the rms amplitudes are quite different in the three independent crystal directions which gives an indication of the crystal anisotropy. The ratio of the ground state rms translational displacement to the intermolecular distance R_{nn} is $< u_a^2 + u_b^2 + u_{c_\perp}^2 >^{1/2} / R_{nn} = 0.056$, which is near twice as large as for solid N_2 [16].

The librational states of the molecules are rather localized in α- and β-O_2 and look like

Table

Translational and librational amplitudes in α- and β-O_2

α-O_2				β-O_2			
Parameter	Value	Parameter	Value	Parameter	Value	Parameter	Value
$\langle u_a^2 \rangle^{1/2}$	0.1092 Å[a]		9.1° [b]	$\langle u_{a;b}^2 \rangle^{1/2}$	0.1200 Å[c]		10.4° [d]
$\langle u_b^2 \rangle^{1/2}$	0.1115 Å[a]	$\langle \vartheta^2 \rangle^{1/2}$	10.84° [a]			$\langle \vartheta^2 \rangle^{1/2}$	11.164° [c]
$\langle u_{c_\perp}^2 \rangle^{1/2}$	0.0889 Å[a]		12.8° [e]	$\langle u_{c_\perp}^2 \rangle^{1/2}$	0.0940 Å[c]		11.6° [f]

[a] Theory [14] for $T = 0$ K.
[b] Experiment [15] for $T = 10$ K.
[c] Theory [14] for $T = 30$ K.
[d] Experiment [15] for $T = 28$ K.
[e] Theory [11] for $T = 10$ K.
[f] Experiment [13] for $T = 30$ K.

weakly anharmonic two-dimensional oscillator states, slightly anisotropic in the case of α-O_2 and isotropic in β-O_2 (Table). The lower frequency in α-O_2 corresponds with libration about the *a* axis, the higher one with libration about the *b* axis. The root-mean-square angular displacements are about 11°, as compared with 16° for α-N_2 at $T = 0$ K [16].

As can be seen from the comparison of the ground state rms amplitudes, translational vibrations in solid oxygen are more anharmonic compared with that in solid nitrogen but for librational vibrations the reverse is true. This difference reflects the distinction in the structures of the intermolecular potentials for the both substances and ultimately the difference in the nature of the stability of α-O_2 and α-N_2 .

The zero-point energy E_{zp} at $P = 0$ for α-O_2 according to Ref. 17 is 204.7 K. Judging from the rms amplitudes obtained in this paper, which are slightly overestimated compared with data from Table, E_{zp} is overestimated as well and should be considered as an upper estimate. The zero-point energy is approximately 20% of the binding energy, of which approximately 40% is due to the librational motion. The high value of the reduced zero-point energy indicates that O_2 displays properties typical for quantum crystals. One of such is a small value of the ratio T_{melt}/Θ_D (T_{melt} is the melting temperature, Θ_D is the Debye temperature), which for solid O_2 is approximately 0.5 (as known, the inequality $T_{\text{melt}}/\Theta_D < 1$ is a signature of a quantum crystal). It is interesting to note that though the reduced value of the zero-point energy for solid N_2 is near the same as that for solid O_2 (see Table 10.1 in Ref. 16), the ratio T_{melt}/Θ_D for solid N_2 is approximately 0.75, markedly higher than for solid O_2 , due to less anharmonic translational vibrations.

The problem of magnetism of solid oxygen turned out to be a considerable challenge. Since in the middle sixties neutron diffraction experiments [2–5] showed unambiguously that α-O_2 is an antiferromagnet, the magnitude of the exchange interaction between oxygen molecules has been a controversial subject of numerous studies. Rather surprising thing is that the first estimates of the exchange field were obtained not from data on the magnetic susceptibility – a property directly connected with the exchange field, but «in a series of elegant experiments» (citing [18]) on the double intramolecular electronic excitation transitions by Eremenko, Litvinenko and co-workers [19–21].

The lowest electron configuration of the oxygen molecule gives rise to three states $^3\Sigma_g^-$, $^1\Delta_g$, $^1\Sigma_g^+$.

Transitions

$$(^3\Sigma_g^-) \rightarrow (^1\Delta_g) \quad 7882 \text{ cm}^{-1},$$

$$(^3\Sigma_g^-) \rightarrow (^1\Sigma_g^+) \quad 13120 \text{ cm}^{-1}$$

are electric dipole forbidden and are very weak. In the condensed phases and in compressed gaseous oxygen, the intensity of these transitions increases significantly. In addition three new absorptions are found and assigned to simultaneous excitation of a pair of oxygen molecules as follows:

$$(^3\Sigma_g^-)(^3\Sigma_g^-) \rightarrow (^1\Delta_g)(^1\Delta_g) \quad 16800 \text{ cm}^{-1},$$

$$(^3\Sigma_g^-)(^3\Sigma_g^-) \rightarrow (^1\Delta_g)(^1\Sigma_g^+) \quad 21000 \text{ cm}^{-1},$$

$$(^3\Sigma_g^-)(^3\Sigma_g^-) \rightarrow (^1\Sigma_g^+)(^1\Sigma_g^+) \quad 27700 \text{ cm}^{-1}.$$

Excellent comprehensive spectroscopic studies of these double molecular transitions are presented in papers by Landau et al. [22] and Eremenko et al. [19]. The effects of temperature and impurity (N_2) have been studied by Eremenko, Litvinenko, and Garber [20,21]. An overview of these double transitions are presented in Fig. 5.

To give the interpretation of the obtained spectroscopic data and their connection with the magnitude of the exchange field we will cite the abstract to the paper by Litvinenko, Eremenko, and Garber «Antiferromagnetic ordering effect on the light absorption spectrum by crystalline oxygen» [21]: «The optical double transition spectrum of crystalline oxygen is studied in the frequency range of 15000 to 31000 cm^{-1} at different temperatures (5 to 27 K) and nitrogen concentrations (0 to 40%). A sharp integral intensity decrease of the absorption

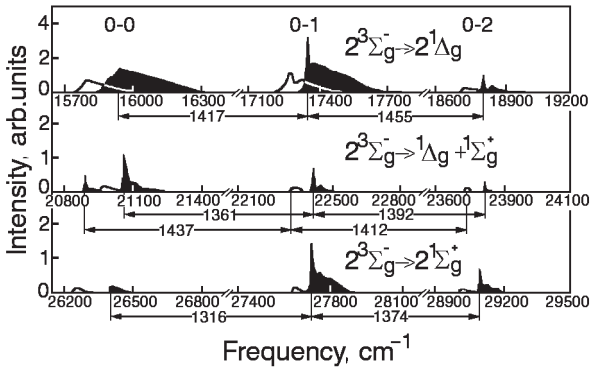

Fig. 5. General view of the light absorption spectrum by solid α-oxygen at $T = 5$ K in the 15000 to 30000 cm^{-1} region: $2^3\Sigma_g^- \rightarrow 2^1\Delta_g$ (v = 0, 1, 2, 3), $2^3\Sigma_g^- \rightarrow {}^1\Delta_g + {}^1\Sigma_g^+$ (v = = 0, 1, 2, 3) and $2^3\Sigma_g^- \rightarrow 2^1\Sigma_g^+$ (v = 0, 1, 2, 3) [21]. The lines at the frequency scale are calculated values for free molecules.

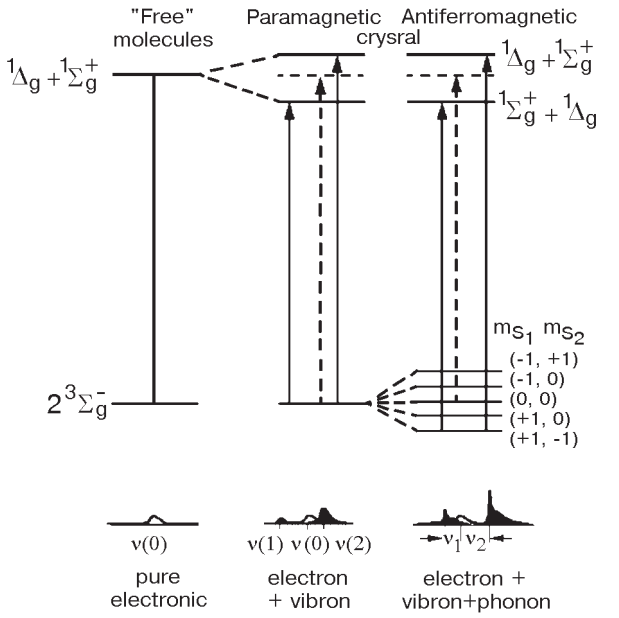

Fig. 6. Energy level diagram of oxygen in the region of a possible vibronic transition in the free molecule as well as in the crystal with magnetic interactions [21].

bands, their shift, and broadening are found in the temperature range investigated. With the insertion of nitrogen into oxygen new absorption bands with spectral positions close to the pure oxygen band frequencies appeared in the oxygen spectrum. The results show that the double transitions in oxygen are considerably induced by exchange interaction. It is also shown that the 0-0 band intensity of the $2^3\Sigma_g^- \to 2^1\Delta_g$ and $2^3\Sigma_g^- \to 2^1\Sigma_g^+$ transitions is determined by the interaction not with acoustic phonons, as it was considered before, but with magnons corresponding to the Brillouin zone boundary and having energy equal to the exchange one $g\mu_B H_E$. The 0-0 band of the $2^3\Sigma_g^- \to 2^1\Delta_g$ and $2^3\Sigma_g^- \to {}^1\Sigma_g^+ + {}^1\Sigma_g^+$ transition is interpreted as a pure electronic band. A consistent scheme, based on considering the exchange splitting of the $^3\Sigma_g^-$ state of the oxygen molecules and the magnon excitation at light absorption is suggested to explain the double transition structures and their band behaviors at magnetic ordering».

In the absence of interaction between a pair of excited molecules, the observed spectrum is simply the sum of the excitations of the two molecules. The perturbations, arising from the molecular interactions (Coulomb-, exchange-, molecular type) remove the degeneracy, strengthen the corresponding transition, produce splitting, and frequency shifts (Fig. 6). The shift decreases with temperature, and also with increasing concentration of N_2. The exchange energy, as measured by the magnon shift, is constant up to 10 K and then falls off smoothly with increasing temperature to about 85% of its low-temperature value before falling rapidly to zero at the α–β transition.

The series of papers [19–21] had a pronounced impact on studies of magnetical and optical properties of solid oxygen. A large number of experimental and theoretical works published in the seventies and subsequent years (see, for instance, [18,23–30]) were directly inspired by results of the magnetooptical studies by Eremenko et al. Effects found in these studies and their interpretation are still the subject of a great interest for investigators (see [31–33]).

3. Librons

First Raman studies of condensed oxygen were made by Cahill and Leroi [15]. In the lattice frequency range they found (Fig. 7) one strong line in the β phase (at ≈ 51 cm^{-1} at 28 K), and two lines in the α phase (at ≈ 43 cm^{-1} and ≈ 78 cm^{-1} at 22 K).

In accordance with the correlation diagram Fig. 8, they assigned the line at 51 cm^{-1} in β-O_2 to the two-fold degenerate E_g libration and the low frequency band in α-O_2 to the B_g libration (libration around the **a** axis and the higher fre-

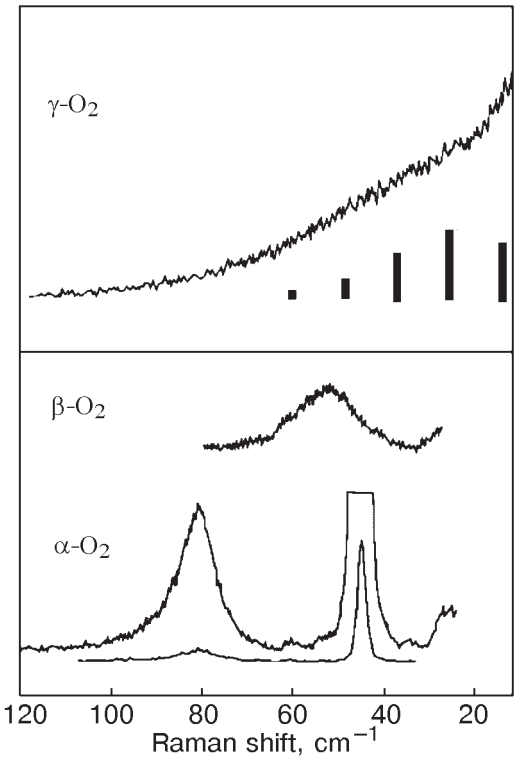

Fig. 7. Raman spectra of α-, β- and γ-oxygen in the low frequency region. Different spectra monitored with different resolutions. Vertical lines are contributions from freely rotating oxygen molecules at $T = 48$ K [15].

Activity	α-O_2 (C_{2h})	Gas ($D_{\infty h}$)	β-O_2 (D_{3d})	Activity
R	A_g	$\Sigma_g^+(\nu)$	A_{1g}	R
R	B_g	$\Pi_g(R_x,R_y)$	E_g	R
ir	B_u	$\Sigma_u^+(T_z)$	A_{2u}	ir
ir	A_u	$\Pi_u(T_x,T_y)$	E_u	ir

Fig. 8. Correlation diagrams for α- and β-oxygen [15].

quency one to the A_g libration (libration around the **b** axis).

Mathai and Allin [25] in the Raman study of α-$^{16}O_2$ and α-$^{18}O_2$ isotopes confirmed the Cahill and Leroi's assignment but found that the isotope shift of the both modes were only about two thirds of that to be expected on the basis of the inverse ratio of the square roots of the reduced masses. The discrepancy was attributed to differences in the anharmonicity of the two isotopes.

There was a long discussion in literature concerning the assignment of the 43 and 78 cm^{-1} lines in the Raman spectra of α-O_2 [1,7,12,17,34]. On the basis of lattice dynamics calculations these authors have cast doubts on the assignment by Cahill and Leroi [15] of these lines as librons. As followed from these lattice dynamics calculations based on different models of the anisotropic forces, at the β–α transition the libron spectrum is only insignificantly changed. The lowering symmetry at this transition leads to removal of the two-fold degeneracy of the frequency of the libron mode $\mathbf{k} = 0$ with a splitting of a few cm^{-1}. At the same time, according to Raman data [15], the doubly degenerate E_g mode of β-O_2 with frequency ≈ 51 cm^{-1} is splitted into B_g and A_g modes with frequencies 43 and 78 cm^{-1}, respectively. According to these authors, the experimentally observed Raman line at 78 cm^{-1} could be a two-particle either magnon-libron [1,7] or two-libron [12,17,34] line while the B_g and A_g splitting is not resolved. Etters et al. [34] have proposed that the higher frequency belongs to a libron mode which lies at the edge of the Brillouin zone for the structural lattice, but which has $\mathbf{q} = 0$ in the magnetic Brillouin zone. This mode could become visible in Raman spectroscopy when there is a strong coupling between the librons and spins. The weakest point of all these interpretations is, however, that under various temperatures and pressures no indication of the doublet character of the lowest peak α-O_2 has been observed.

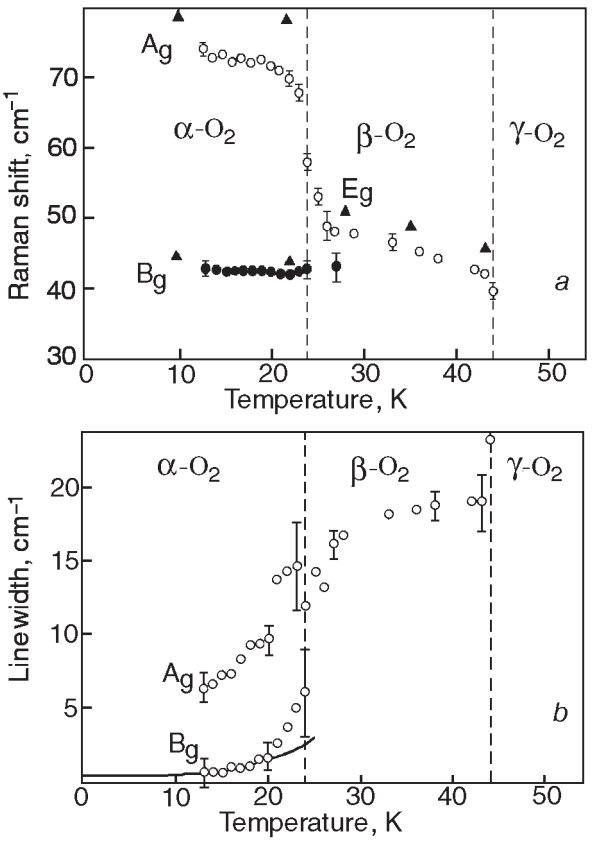

Fig. 9. Temperature dependence of the librational frequencies (*a*) and bandwidth (*b*) of solid oxygen (▲ from [15]) [35].

Subsequent experimental and theoretical studies gave an insight into what really happens with the libron spectrum under the α–β transition. Measurements by Bier and Jodl [35] and by Prikhot'ko et al. [36] have given a strong evidence that the assignment by Cahill and Leroi [15] is correct (Fig. 9,*a*).

The experimental data indicate that the upper A_g mode exhibits a typical soft-mode behavior and at the α–β transition transforms into E_g mode of the β phase. The intensity and linewidth of the A_g mode increases rapidly in the vicinity of the transition and go over continuously to the respective characteristics of the E_g mode (Fig. 9,*b*). The B_g mode frequency is nearly constant with temperature but its intensity decreases rapidly when nearing the phase transition point, and the line vanishes discontinuously after passing the phase transition.

From the theoretical side, Krupskii et al. [1] suggested that the large splitting of the libron spectrum at the β–α transition could be due to an additional term in the libron Hamiltonian, which is proportional to the magnetic order parameter. Since for $T > T_{\alpha-\beta}$ the magnetic order parameter turns to zero, this term is nonvanishing only in the α phase. Jansen and van der Avoird [37,14] found

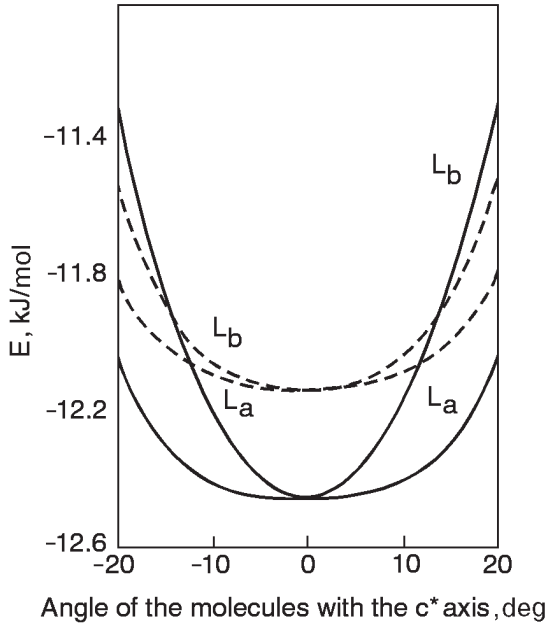

Fig. 10. The plot of the lattice potential of α-O_2 along the normal coordinates for the B_g and A_g librons, with (solid curves) and without (dashed curves) the contribution of the Heisenberg term [14].

that because of the very strong dependence of the exchange coupling parameter on the molecular orientations the Heisenberg term from the spin Hamiltonian should be included in the libron spectrum calculations.

The plot of the lattice potential along the normal coordinates for the B_g and A_g librons, with and without the contribution of the Heisenberg term, clearly demonstrates its role in this problem (Fig. 10 [14]). This term lowers the lattice energy of α-O_2 at the equilibrium geometry. At the same time it drastically increases the stiffness of the potential in the A_g direction, but much less in the B_g direction.

An integrated formalism that includes magnon–phonon and magnon–libron coupling in dynamics of orientationally ordered α and β phases of solid oxygen was developed by Jansen van der Avoird [14] on the base of the time-dependent Hartree method (random phase approximation). We will consider the problem of magnon–libron coupling following a more simple approach of Refs. 38, 39.

The intermolecular exchange constant can be written as a sum of a part, which is independent of the orientations of the O_2 molecules and an orientationally dependent term. The latter part contributes to the anisotropic intermolecular potential, which determines the spectrum of librons in the orientationally ordered α and β phases. Both the exchange part and the spin independent part of the intermolecular potential may be written as a sum of products of invariants $(\boldsymbol{\Omega}_1\mathbf{n})$, $(\boldsymbol{\Omega}_2\mathbf{n})$, $(\boldsymbol{\Omega}_1\boldsymbol{\Omega}_2)$:

$$U(\boldsymbol{\Omega}_1,\boldsymbol{\Omega}_2,\mathbf{R}) = \sum_{i,k,l} A_{ikl}(R)(\boldsymbol{\Omega}_1\mathbf{n})^i(\boldsymbol{\Omega}_2\mathbf{n})^k(\boldsymbol{\Omega}_1\boldsymbol{\Omega}_2)^l, \quad (1)$$

$$J(\boldsymbol{\Omega}_1,\boldsymbol{\Omega}_2,\mathbf{R}) = \sum_{i,k,l} B_{ikl}(R)(\boldsymbol{\Omega}_1\mathbf{n})^i(\boldsymbol{\Omega}_2\mathbf{n})^k(\boldsymbol{\Omega}_1\boldsymbol{\Omega}_2)^l, \quad (2)$$

where i, k, l are integers, the pairwise sums of which are even numbers; A_{ikl}, B_{ikl} are expansion coefficients, which are functions of molecular parameters and intermolecular distance R. Here $\boldsymbol{\Omega}_1$, $\boldsymbol{\Omega}_2$ are unit vectors along the molecular axis, $\mathbf{R}$ is the vector joining molecular centers, $\mathbf{n} = \mathbf{R}/R$. The anisotropic parts can obtained from the expansions of Eqs. (1), (2) after excluding the terms with $i + k + l = 0$, which corresponds to the isotropic parts of the exchange constant and spin-independent intermolecular potential. In fact, the representation of the Kohin potential [16] is an example of the expansion Eq. (1) up to terms with $i + k + l \le 3$, which includes all terms necessary for the derivation of the harmonic approximation.

Taking into account the explicit form of the exchange intermolecular interaction and averaging Eq. (2) over the ground spin state, we can obtain the total anisotropic intermolecular interaction $(V_{\text{anis}}(\boldsymbol{\Omega}_1,\boldsymbol{\Omega}_2,\mathbf{R}))$, which can be written a sum of the spin-independent and spin-dependent contributions:

$$V_{\text{anis}}(\boldsymbol{\Omega}_1,\boldsymbol{\Omega}_2,\mathbf{R}) =$$

$$= U_{\text{anis}}(\boldsymbol{\Omega}_1,\boldsymbol{\Omega}_2,\mathbf{R}) + J_{\text{anis}}(\boldsymbol{\Omega}_1,\boldsymbol{\Omega}_2,\mathbf{R})\langle \mathbf{S}_1\mathbf{S}_2\rangle, \quad (3)$$

Where $\langle \mathbf{S}_1\mathbf{S}_2\rangle$ is the spin correlation function. Finally we have

$$V_{\text{anis}}(\boldsymbol{\Omega}_1,\boldsymbol{\Omega}_2,\mathbf{R}) =$$

$$= \sum_{\substack{i,k,l \\ i+k+l\neq 0}} (A_{ikl} + B_{ikl}\langle \mathbf{S}_1\mathbf{S}_2\rangle)(\boldsymbol{\Omega}_1\mathbf{n})^i(\boldsymbol{\Omega}_2\mathbf{n})^k(\boldsymbol{\Omega}_1\boldsymbol{\Omega}_2)^l. \quad (4)$$

As can be seen from Eq. (4), the anisotropic intermolecular potential, which determines the spectrum of librons in the orientationally ordered α and β phases, contains the additional term, which depends on the character and value of the magnetic order. In the molecular field approximation we have that in the β phase $\Gamma_{\mathbf{mn}} = \langle \mathbf{S_m}\mathbf{S_n}\rangle = 0$ and in the α phase for the nearest molecules from the different sublattices $\Gamma_{\mathbf{mn}} = -s^2$, where s is the average spin. For the ordered three-sublattice magnetic structure we would have $\Gamma_{\mathbf{mn}} = -s^2/2$, which can

serve as an estimate of the spin correlation function for the case of the short magnetic order.

The expansion coefficients A_{ikl}, B_{ikl} are generally speaking of the same order of magnitude, which means that the additional term cannot be treated as a small perturbation but should be taken into account in the zero approximation.

The system of interacting rotors is described by the Hamiltonian

$$\mathcal{H} = \mathcal{H}_{\text{kin}} + V_{\text{anis}}, \tag{5}$$

where the kinetic energy operator is

$$\mathcal{H}_{\text{kin}} = -B_{\text{rot}} \times$$
$$\times \sum_{\mathbf{f}} \left(\frac{1}{\sin \vartheta_{\mathbf{f}}} \frac{\partial}{\partial \vartheta_{\mathbf{f}}} \sin \vartheta_{\mathbf{f}} \frac{\partial}{\partial \vartheta_{\mathbf{f}}} + \frac{1}{\sin^2 \vartheta_{\mathbf{f}}} \frac{\partial^2}{\partial \varphi_{\mathbf{f}}^2} \right). \tag{6}$$

Here $B_{\text{rot}} = \hbar^2/2I$ (I is the molecular moment of inertia) is the characteristic rotational constant; $\vartheta_{\mathbf{f}}$ and $\varphi_{\mathbf{f}}$ are the angles determining the molecular orientation at site $\mathbf{f}$.

Since $B_{\text{rot}} << V_{\text{anis}}$, the rotor wave functions have localized near $\vartheta = 0$, that is the anharmonic terms are small and librons are well-defined quasiparticles. Retaining in the Hamiltonian Eq. (5) only harmonic terms and neglecting the interplane interaction, we obtain for the frequencies of librons in α- and β-O_2 in the center of the Brillouin zone the following expressions:

β-O_2:
$$(\hbar\Omega_{E_g})^2 = 6B_{\text{rot}} \times$$
$$\times \left\{ (2A_{200}^{\beta} + A_{111}^{\beta}) + (2B_{200}^{\beta} + B_{111}^{\beta})\Gamma^{\beta} \right\}; \tag{7}$$

α-O_2:
$$(\hbar\Omega_{A_g})^2 = 6B_{\text{rot}} \times$$
$$\times \left\{ (2A_{200}^{1\alpha} + A_{111}^{1\alpha}) + (2B_{200}^{1\alpha} + B_{111}^{1\alpha})\Gamma_1^{\alpha} \right\}; \tag{8}$$

$$(\hbar\Omega_{B_g})^2 = B_{\text{rot}} \times$$
$$\times \left\{ 4\left(A_{200}^{1\alpha} + 2A_{200}^{2\alpha}\right) + 2\left(A_{111}^{1\alpha} + 2A_{111}^{2\alpha}\right) + \right.$$
$$\left. + 2\left(2B_{200}^{1\alpha} + B_{111}^{1\alpha}\right)\Gamma_1^{\alpha} + 4\,(2B_{200}^{2\alpha} + B_{111}^{2\alpha})\Gamma_2^{\alpha} \right\}, \tag{9}$$

where A_{ikl}^{β}, B_{ikl}^{β} are values of respective parameters of the intermolecular potential for the intermolecular distances in the β phase; $A_{ikl}^{1\alpha}$, $B_{ikl}^{1\alpha}$ and $A_{ikl}^{2\alpha}, B_{ikl}^{2\alpha}$ are values of respective parameters of the intermolecular potential for the intermolecular distances in the α phase for the nearest neighbors from the opposite and the same magnetic sublattices, respectively; Γ^{β} is the spin correlation function for two nearest spins in the β phase; $\Gamma^{1\alpha}, \Gamma^{2\alpha}$ are the spin correlation functions in the α phase for two nearest neighbors from the opposite and the same sublattices, respectively.

Neglecting the small monoclinic distortion at the α–β transition, that is, the small difference between $A_{ikl}^{1\alpha}$, $A_{ikl}^{2\alpha}$, and A_{ikl}^{β} (and the same for the B_{ikl} parameters), we can simplify Eqs. (7)–(9):

$$(\hbar\Omega_{E_g})^2 = 6B_{\text{rot}} \times$$
$$\times \left\{ (2A_{200} + A_{111}) + (2B_{200} + B_{111})\Gamma^{\beta} \right\}; \tag{10}$$

$$(\hbar\Omega_{A_g})^2 = 6B_{\text{rot}} \times$$
$$\times \left\{ (2A_{200} + A_{111}) + (2B_{200} + B_{111})\Gamma_1^{\alpha} \right\}; \tag{11}$$

$$(\hbar\Omega_{B_g})^2 = 6B_{\text{rot}} \times$$
$$\times \left\{ (2A_{200} + A_{111}) + \frac{1}{3}(2B_{200} + B_{111})(\Gamma_1^{\alpha} + 2\Gamma_2^{\alpha}) \right\}. \tag{12}$$

Equations (7)–(9) and (10)–(12) provide an explanation of the main anomaly features of the temperature dependence of librons in α and β phases (Fig. 9,*a*) – large and strongly asymmetric splitting, a strong temperature dependence of the A_g mode and a week temperature dependence of the B_g mode.

According to data from Raman scattering spectra [15,35], at the α–β transition the two-fold degeneracy of the libron spectrum is lifted and the doubly degenerate E_g mode of β-O_2 with frequency ~ 51 cm^{-1} is splitted into the B_g and A_g modes with frequencies ~ 43 and ~ 78 cm^{-1}. The reconstruction of the structure accompanying the phase transition and the related changes in the anisotropic part of the intermolecular potential cannot be the reason of such large splitting. If we disregard terms proportional to Γ in Eqs. (7)–(9), the resulting splitting of the E_g mode is

$$\Delta = \frac{B_{\text{rot}}}{\hbar\Omega_{E_g}} \left[2(A_{200}^{2\alpha} - A_{200}^{1\alpha}) + (A_{111}^{2\alpha} - A_{111}^{1\alpha}) \right]. \tag{13}$$

Estimates were obtained $\Delta < 5$ cm^{-1} [1,7,12].

As follows from Eqs. (10)–(12), the large splitting is completely due to the spin-libron interaction:

$$\Delta = \frac{2B_{\text{rot}}}{\hbar\Omega_{E_g}} (2B_{200} + B_{111})(\Gamma_1^{\alpha} - \Gamma_2^{\alpha}). \tag{14}$$

Other anomaly features of the libron spectrum are also due to the spin-libron interaction. The displacements $\Delta A_g = (\Omega_{A_g} - \Omega_{E_g})$, $\Delta B_g = (\Omega_{E_g} - \Omega_{B_g})$ of the A_g

and B_g modes respective the E_g mode of β-O_2 can be found from the following equations:

$$(\hbar\Omega_{A_g})^2 - (\hbar\Omega_{E_g})^2 = \\ = 6B_{\rm rot}(2B_{200} + B_{111})(\Gamma_1^\alpha - \Gamma^\beta); \quad (15)$$

$$(\hbar\Omega_{E_g})^2 - (\hbar\Omega_{B_g})^2 = \\ = 6B_{\rm rot}(2B_{200} + B_{111})\left[\Gamma^\beta - \frac{1}{3}(\Gamma_1^\alpha + 2\Gamma_2^\alpha)\right]. \quad (16)$$

In a general theory the spin correlation functions should be found in a self-consistent way together with the libron spectrum, but as a zero approximation they could be found independently from the spin Hamiltonian. The following estimates can be obtained:

$$\left|\Gamma^\beta\right| << \left|\Gamma_1^\alpha\right|, \left|\Gamma_2^\alpha\right|; \quad (17)$$

$$\left|\Gamma_1^\alpha + 2\Gamma_2^\alpha\right| << \left|\Gamma_1^\alpha\right|, \left|\Gamma_2^\alpha\right|. \quad (18)$$

As follows from Eqs. (15), (16) and inequalities Eqs. (17), (18), $\Delta B_g << \Delta A_g$, that is, the splitting is strongly asymmetric around Ω_{E_g}.

This asymmetry can be understood qualitatively as follows [40]. When the molecules librate around the **b** axis (A_g symmetry) the interaction with four nearest-neighbor molecules from the opposite magnetic sublattice, is mostly involved, but when they librate around the **a** axis (B_g symmetry) the interaction with two next-nearest-neighbor molecules from the same magnetic sublattice is involved. The latter is much weaker than for the A_g librational mode. As a result, $\Delta B_g << \Delta A_g$.

The variation of the libron frequencies with temperature are caused by three factors: first, there are anharmonic temperature shifts of the frequencies with temperature, second, the parameters A_{ikl} , B_{ikl} vary with temperature due to the thermal expansion of the lattice, and third, due to the temperature dependence of the spin correlation functions $<\mathbf{S}_i\mathbf{S}_j>$. In the case of the α phase, the latter factor is most important. In the case of the β phase, the temperature shift of the E_g mode is mostly determined by the thermal expansion of the lattice. The resulting temperature dependence can be written in the form

$$\left(\frac{\partial\Omega}{\partial T}\right)_P = \left(\frac{\partial\Omega}{\partial T}\right)_V + \left(\frac{\partial\Omega}{\partial V}\right)_T \left(\frac{\partial V}{\partial T}\right)_P. \quad (19)$$

Anharmonic corrections to the librational frequencies of the β phase was calculated in the mean-field approximation in Ref. 13. The anharmonicity is manifested in the explicit temperature dependence of the librational frequencies. It was shown, that contrary to solid N_2 the sign of the anharmonic correction in β-O_2 is positive. Since $(\partial\Omega/\partial T) = (\partial\Omega/\partial\eta)(\partial\eta/\partial T)$ while $(\partial\eta/\partial T) < 0$ (where η is the orientational order parameter), the sign of the anharmonic correction is determined by the sign of the derivative $(\partial\Omega/\partial\eta)$, which could be either positive or negative, depending on signs and values of molecular and crystal field constants in the self-consistent potential. As a result, in the case of β-O_2 the derivative $(\partial\Omega/\partial\eta) < 0$ and $(\partial\Omega/\partial T) > 0$. As shown by numerical estimates, $(T/\Omega)(\partial\Omega/\partial T) \approx 10^{-3}$ and the effect is dominated by the second term in Eq. (19), the thermal expansion of the crystal. The comparison of the calculated [1] and experimental dependencies of the E_g frequency on temperature is given in Fig. 11.

The effect of an external magnetic field on the libron spectrum of α- and β-O_2 was calculated by Jansen and van der Avoird [14]. They predicted that the libron frequencies will be shifted by the external magnetic field, which changes the spin correlation function and according to Eq. (4) affects the anisotropic part of the intermolecular potential. Due to high rigidity of the magnetic structure of α-O_2, the resulting shift of A_g and B_g librons is small even in strong fields and amount to 2.5 cm^{-1} for fields up to 30 T (Fig. 12,*a*). The magnetic field induced shift of the E_g mode for β-O_2 is given in Fig. 12,*b*.

When the magnetic field is parallel to the *ab* plane of the β phase one might expect several symmetry-breaking effects [14]. The threefold symmetry is distorted in this case with the result that the E_g mode will be slightly splitted.

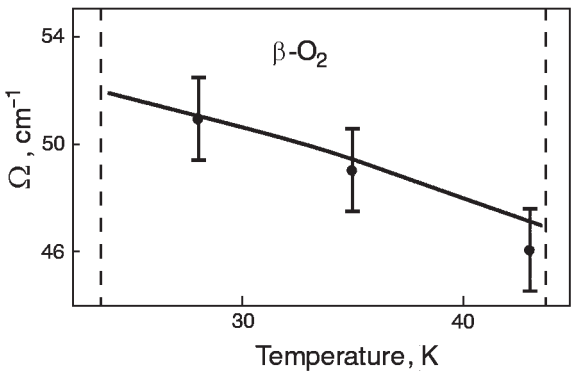

Fig. 11. Temperature dependence of the frequency of the E_g libron mode of β-O_2 . Solid line are theoretical results from Ref. 1, solid circules are experimental data Ref. 15.

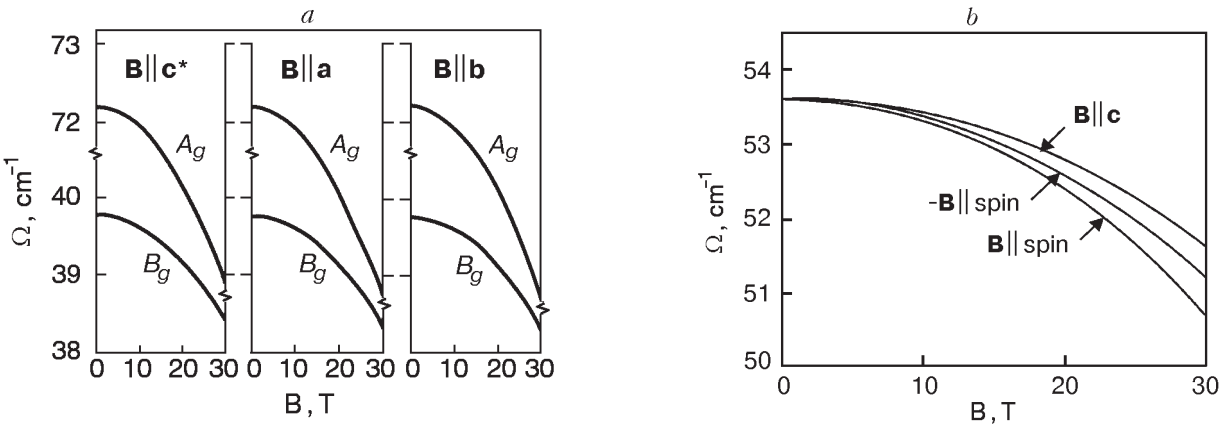

Fig. 12. The magnetic field induced shift of the A_g and B_g librons in α-O_2 (*a*) and the E_g libron mode in β-O_2 (*b*) [14].

Due to the zone-folding effect, extra phonon or libron peaks may become visible in the IR or Raman spectra though their intensities are predicted to be small.

4. Translational phonons

The magnon–phonon coupling leads to the zone folding [38]: the magnetic unit cell contains two molecules, and as a result, in the folded zone the phonon zone subdivided into acoustical and optical phonons and the number of libron and magnon branches is doubled.

The most extensive zero-temperature lattice dynamics harmonic calculations based upon both the one-molecular crystallographic unit cell and the two-molecular magnetic cell have been made by Etters et al. [34]. At the first step the Gibbs free energy was minimized with the parameters of the monoclinic lattice cell of α-O_2 and the intramolecular bond length as independent variable parameters. Using obtained equilibrium lattice parameters harmonic lattice-dynamics calculations have been made. The calculations were based on the site-site Etters–Kobashi–Belak (EKB) potential [34]. Since the strong anisotropy of the Heisenberg term are not taken into account in the EKB potential, the calculated dispersion curves suffer from the same shortcomings as all older lattice dynamics calculations and reproduce the libron modes incorrectly. Nontheless, many qualitative results of these calculations retain its validity.

The magnetic unit cell contains two molecules in the unit cell, twice as large as the structural unit cell. There are six phonon modes, four libron modes, and four magnon modes for every wave vector **q** in the smaller Brillouin zone, that is, compared with the crystallographic cell, magnetic unit cell supports one additional vibron, two additional libron modes, three additional optical phonon modes and two additional magnon modes. The problem is that none of these modes were observed in experiment. Recently, the range 10–85 cm^{-1} was investigated very carefully by Medvedev [31] using the modern FTIR technique and perfect crystals, and no additional IR-active modes were found.

The integrated lattice dynamics calculations in the random phase approximation have been made by Jansen and van der Avoird [14]. It was found that the mixing between the lattice modes, phonons and librons, and magnons, is in general, small. The only substantial amount of mixing occurs in those regions of the Brillouin zone where the dispersion curves for the lattice modes and those for the magnons would cross. Even the weak coupling then leads to an avoided crossing and to interchange of character of the modes involved.

The translational lattice frequencies for the orientationally disordered γ-O_2 have been calculated by Kobashi, Klein, and Chandrasekharan [12] using different empirical Lennard-Jones (6–12) intermolecular potentials to account for the interactions between nearest discs, between the nearest disc and sphere and between the second nearest discs. The model completely neglects the effect of molecular rotation. The model was able to account for the low shear constant of γ-O_2, but considerably overestimated the elastic anisotropy. This discrepancy was attributed to the neglect of translation–rotation coupling.

The role played by the molecular reorientational motions in the crystal dynamics of γ-O_2 was examined by Klein, Levesque, and Weis [41] in a molecular dynamics study of a system of molecules interacting via atom-atom potential. The simulated crystal revealed two types of molecules with two

quite different types of dynamical behavior. Very slow transverse acoustic phonon modes were found with $v_l/v_t \approx 3.5$ in a fair agreement with experiment [42,43]. The liquid has been shown to be very similar in structure and dynamical behavior to the γ phase.

5. Magnons

The first observation of the resonant FIR absorption in α-O_2 was made by Blocker, Kinch, and West [23]. They found a strong line at about 27 cm^{-1} with the linewidth of about 1.4 cm^{-1} and attributed it to the antiferromagnetic resonance (AFMR) mode of the system. This peak shifts to lower frequencies and decreases markedly in intensity with increasing temperature and is unobserved above the α–β transition (Fig. 13,*a*). The experimental proof of the magnon nature of the line was obtained by Wachtel and Wheeler [18,24] who demonstated that no detectable isotopic effect was observed. The temperature dependence of the high energy magnon was studied by several groups ([23,30,44]) with similar results.

Looking for the low-frequency AFMR line Wachtel and Wheeler [24] found an absorption line at 6.4 cm^{-1} at 1.5 K (Fig. 13,*b*). To support the assignment of the found FIR absorption lines as AFMR modes, FIR spectra were measured as a function of applied megnetic field [18,24,44,45].

The dispersion relations for magnons in the presence of the magnetic field were calculated in Refs. 24, 45–47. A comparison of experimental and calculated results is given in Fig. 14 [45]. The experimental absorption band corresponding to the low-energy magnon is splitted: one absorption maximum does not shift when the field increases, and the frequency of another increases with the field (Fig.14,*a*). In the case of the high-energy magnon the splitting was not found (Fig. 14,*b*).

Experimental results of Refs. 18–21, 23–25 provided an experimental basis for the development of theory of the magnetic properties of solid oxygen and first of all of the spin excitation spectrum.

The magnetic properties of solid oxygen is generally described by the Hamiltonian [17,18,24,29, 45–50]

$$\mathcal{H} = \sum_{\mathbf{f}} [A(S_{\mathbf{f}}^z)^2 + B(S_{\mathbf{f}}^y)^2] + \frac{1}{2}\sum_{\mathbf{f},\mathbf{f}'} J_{\mathbf{ff}'}\mathbf{S}_{\mathbf{f}}\mathbf{S}_{\mathbf{f}'}, \quad (20)$$

where $\mathbf{S}_{\mathbf{f}}$ is the spin operator at site $\mathbf{f}$ ($S = 1$), A > 0 and $B > 0$ are constants of single-molecule anisotropy, and $J_{\mathbf{ff}'}$ is the exchange interaction constant of molecules at sites $\mathbf{f}$ and $\mathbf{f}'$. The z axis in Eq. (20) coincides with the molecular axis, while the x axis is directed along the monoclinic **b** axis.

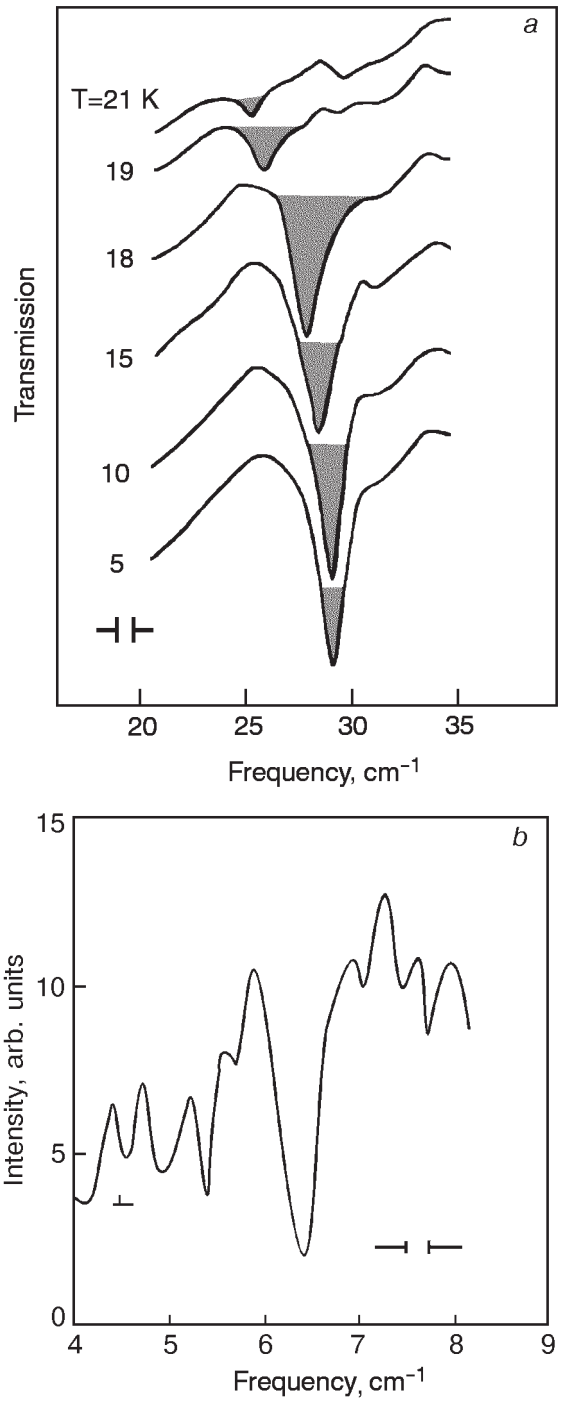

Fig. 13. Spectroscopic proof of magnon excitations in solid oxygen. The temperature dependence of far IR absorption due to magnon excitation at 27 cm^{-1} in solid oxygen [23] (*a*). The magnon at 6 cm^{-1} is clearly recognizable in far IR absorption spectra of solid oxygen [24] (*b*).

The first calculation of the spin excitation spectrum was done by Wachtel and Wheeler [18,24]. According to the usual excitation wave method, the diagonalization of the Hamiltonian (20), was per-

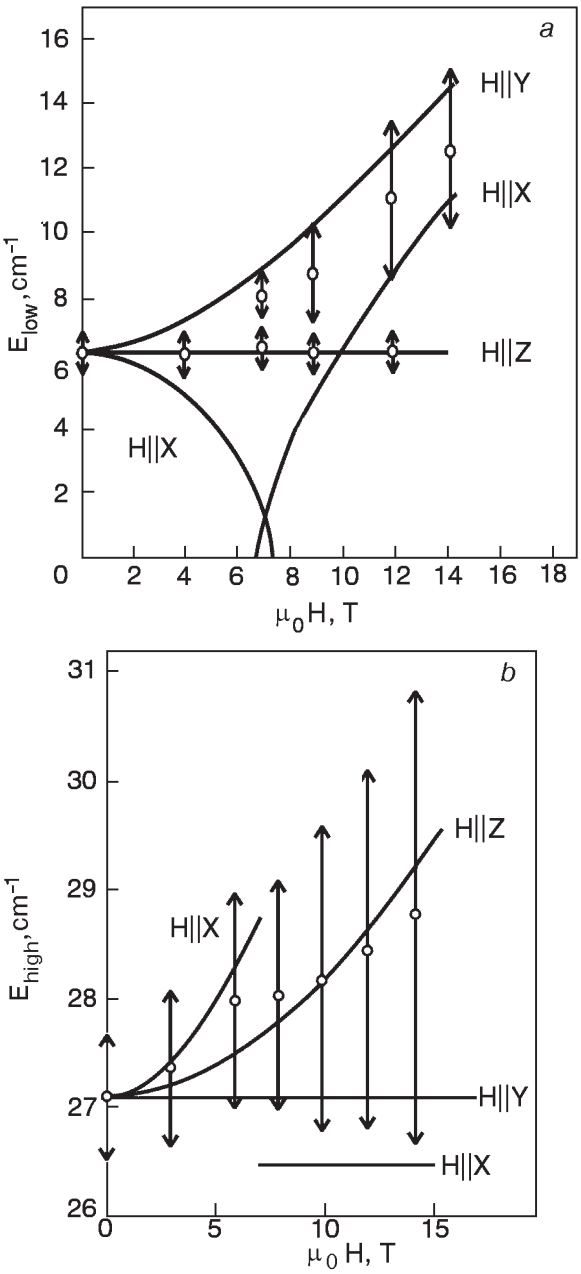

Fig. 14. Magnetic-field dependence of the frequency of the low-energy (*a*) and high-energy (*b*) magnons, measured on polycrystalline samples of α-O_2 . Experimental absorption maxima are represented by open dots, vertical arrors indicate the FWHM (full width at half maximum). The $H||X$ curve starting at $H = 0$ corresponds to the non-spin-flopped phase, the other $H||X$ curve corresponds to the spin-flopped phase [45].

formed in two steps. First, the Hamiltonian (20) was written as a sum of a single-particle mean-field Hamiltonian $\mathcal{H}_0$

$$\mathcal{H}_0 = \sum_i (AS_{zi}^2 + BS_{yi}^2 + J(0) < S_x > S_{xi}) \quad (21)$$

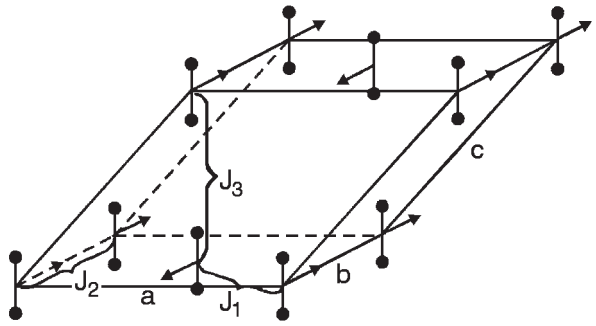

Fig. 15. Monoclinic structure of α-O_2. The magnetic structure is indicated by the arrows. The exchange interaction between the in-plane and out-of-plane neerest neighbors is described by the respective exchange interaction constants J_1 , J_2 , J_3 .

and the interaction Hamiltonian $\mathcal{H}_{\text{int}} = \mathcal{H} - \mathcal{H}_0$, where $< S_x >$ is the expectation of the operator S_x in the single molecule ground state, which should be found from self-consistency conditions. Here the direction of the moments (b axis) is taken as the axis of spin quantization. The exchange field $J(0) = J(\mathbf{k} = 0)$; $J(\mathbf{k}) = \sum_{\delta} J_{\mathbf{f},\mathbf{f}+\delta} e^{i\mathbf{k}\delta}$ is the magnetic structure factor, δ are lattice vectors.

With account of nearest, next nearest and next-next neighbors we have the following expression for the exchange field:

$$J(0) = n_1 J_1 - n_2 J_2 + n_3 J_3 \ , \quad (22)$$

where n_1 , n_2 , n_3 are numbers of the respective neighbors ($n_1 = 4$, $n_2 = 2$, $n_3 = 4$) and J_1 , J_2 , J_3 are respective exchange constants (see Fig. 15).

As a result, the magnetic structural factor for the α-oxygen structure can be written in the form

$$J(\mathbf{k}) = J(0)\gamma_{\mathbf{k}};$$

$$\gamma_{\mathbf{k}} = \frac{1}{1 - \kappa/2 + \alpha} \times$$

$$\times \left[\cos\frac{k_x}{2} \cos\frac{k_y}{2} - \frac{1}{2}\kappa \cos k_y + \alpha \cos\frac{k_y}{2} \cos(\frac{k_x}{2} - k_z) \right], \quad (23)$$

where two dimensionless parameters $\alpha = J_2/J_1$ and $\kappa = J_3/J_1$ were introduced. Thus, neglecting the interaction with more distant neighbors the magnetic Hamiltonian (20) is described by the set of 5 parameters: J_1, α, κ, A, B.

The eigenvalue problem for $\mathcal{H}_0$ can be solved in a straightforward manner, yielding the following eigenvalues:

$$\epsilon_{\substack{0\\2}} = \frac{A+B}{2} \mp \sqrt{\left(\frac{A-B}{2}\right)^2 + J^2(0) < S_x >^2}; \qquad (24)$$

$$\epsilon_1 = A + B$$

(ϵ_0 is the ground state energy, ϵ_1 , ϵ_2 are the first and second excited states, respectively). The resulting eigenfunctions then used as the basis for transformation of the Hamiltonian $\mathcal{H} = \mathcal{H}_0 + \mathcal{H}_{\rm int}$ into second quantized representation in terms of fermion creation and annihilation operators $c_{fi}^{\dagger}, c_{fi}$. Different approaches and approximations of the excitation wave method [1,7,18,24,29,45–49] and of the Green function method [46,48] were used to treat the problem.

At low temperatures the occupation number of the ground state $n_{f0} = c_{f0}^{\dagger} c_{f0}$ is close to unity. In this limit terms not quadratic in ground state may be neglected (so-called Bogolyubov approximation). Introducing the product operators $a_{fi}^{\dagger} = c_{fi}^{\dagger} c_{f0}$ and $a_{fi} = c_{f0}^{\dagger} c_{fi}$, which approximately obey the Bose commutation relations, and transforming the Hamiltonian to these operators, we obtain the Hamiltonian quadratic in Bose excitation operators. The next simplification consists in neglecting excitations from the ground state to the second excited state. The resulting dispersion relations (energy vs quasimomentum relations) can be written in the form:

$$E_n^2(\mathbf{k}) = [\Delta_{10} + (-1)^n J(\mathbf{k}) \sin 2\vartheta]^2 - J^2(\mathbf{k}); \; n = 1; 2, \qquad (25)$$

where $\Delta_{10} = \epsilon_1 - \epsilon_0$ is the energy necessary to excite the molecule from the ground state to its first excited state; ϵ_0 , ϵ_1 are given by Eq. (24); ϑ is a mixing parameter which determines the ratio of $|+1\rangle$ and $\langle -1|$ in the ground state. It depends on the relative magnitudes of the anisotropy parameters A and B:

$$\tan 2\vartheta = (A - B)/[2J(0) < S_x >] \; . \qquad (26)$$

It is important to note that because of complexity of the commutation relations for spin operators, there is no single «true» dispersion equation which would be independent of the way of transformation of the spin Hamiltonian into the bosonic Hamiltonian and of subsequent approximations used for its diagonalization. All these approaches are so-called uncontrollable approximations contrary to a few controllable ones (among these are the high-temperature expansions [51] and the low-temperature Dyson approach [52]). That is why, it is important to use different approximations for the derivation of the dispersion equation, and then, comparing magnetic characteristics calculated with different dispersion equations, to decide which approach is preferable.

The simplest approximation not based explicitely on the assumption of small fluctuations of the spin density is the random phase approximation (RPA) coinciding with the Tyablikov approximation [53] in the case of the ordered phase. This approximation was used by Slusarev et al. [49,50] to develop theory of magnetic properties of α and β phases.

After applying the decoupling procedure usual for the RPA approximation, the set of linearized equation of motion in $\mathbf{k}$ space was obtained, where spin components S_x, S_y, S_z are coupled to components of the quadrupole magnetic moment $Q_{ij} = (1/2)(S_i S_j + S_j S_i) - (2/3)\delta_{ij}$ with the result that the order of the system is doubled.

As a result, the following expression was obtained for two lower branches of the spin wave spectrum [49,50]:

$$E_n^2(\mathbf{k}) = \frac{J^2(0)}{2 - \gamma_{\mathbf{k}}^2} \left\{ \eta[1 + (-1)^n \gamma_{\mathbf{k}}] - (-1)^n \frac{2B\xi_1}{\eta J(0)} \gamma_{\mathbf{k}} \right\} \times$$

$$\times \left\{ \eta[1 - (-1)^n \gamma_{\mathbf{k}}] + (-1)^n \frac{2A\xi_2}{\eta J(0)} \gamma_{\mathbf{k}} \right\}; \; n = 1; 2 \; . \qquad (27)$$

Here η is the spin order parameter of the system

$$\eta = \frac{1}{N} \sum_{\mathbf{k}} < S_{\mathbf{k}}^x > \qquad (28)$$

and ξ_1 and ξ_2 are order parameters of quadrupole magnetic ordering:

$$\xi_1 = \frac{1}{N} \sum_{\mathbf{k}} \left(\left\langle S_{\mathbf{k}}^x S_{-\mathbf{k}}^x \right\rangle - \left\langle S_{\mathbf{k}}^z \; S_{-\mathbf{k}}^z \right\rangle \right);$$

$$\xi_2 = \frac{1}{N} \sum_{\mathbf{k}} \left(\left\langle S_{\mathbf{k}}^x S_{-\mathbf{k}}^x \right\rangle - \left\langle S_{\mathbf{k}}^y S_{-\mathbf{k}}^y \right\rangle \right). \qquad (29)$$

The self-consistency parameters are determined by integrals over the Brillouin zone, which makes it possible to neglect anisotropies contributing only to the center and to the band edges. In this approximation $\xi_1 = \xi_2 = \xi$. As follows from Eq. (27), the AFMR frequencies $E_1(0)$, $E_2(0)$ are defined by the exchange field $J(0)$, respective anisotropy constants, and by the quadrupole magnetic order parameter ξ:

$$E_1(0) = \sqrt{4B\xi J(0)}; \; E_2(0) = \sqrt{4A\xi J(0)}. \qquad (30)$$

At $T = 0$ K the order parameters η and ξ satisfy two self-consistency conditions:

$$\xi = 2 - \frac{3}{2}\eta R; \quad \eta = 2\xi R, \tag{31}$$

where

$$R = \frac{1}{N}\sum_{\mathbf{k}} [1 - \gamma^2(\mathbf{k})]^{-1/2} . \tag{32}$$

According to Ref. 54, in the two-dimensional case $R = 1.393$, and in the three-dimensional case $R = 1.156$. The self-consistency parameters η and ξ, determined by the set of equations Eq. (31), equal for 2D and 3D:

$$\text{2D:} \quad \eta = 0.817; \quad \xi = 0.293; \tag{33}$$

$$\text{3D:} \quad \eta = 0.923; \quad \xi = 0.399. \tag{34}$$

In numerical calculations the values of these parameters were used for the two-dimensional case ($\alpha = J_2/J_1 << 1$).

Bearing in mind that we will compare different forms of the dispersion equation obtained in different approximations for the Hamiltonian (20), we will recast Eqs. (25) and (27) in the form more convenient for such comparison.

The dispersion equation (25) has the same total number of parameters as the original magnetic Hamiltonian (20), but the anisotropy parameters A and B enter into Eq. (23) through quantities Δ_{10} and $\sin 2\vartheta$. Appearing of these quantities reflects the way which was used to obtain the dispersion equation in this specific form. They can be expressed in terms of the exchange field $J(0)$, and $E_1(0)$ and $E_2(0)$, frequencies of two AFMR modes. As a result of straightforward transformations, Eq. (25) takes the form

$$E_n(\mathbf{k}) = \left\{ [a_+ + (-1)^n a_- \gamma_{\mathbf{k}}]^2 - J^2(\mathbf{k}) \right\}^{1/2}, \tag{35}$$

where parameters $a_\pm$ are given by

$$a_\pm = \frac{1}{2}\left\{ \sqrt{E_2(0)^2 + J^2(0)} \pm \sqrt{E_1(0)^2 + J^2(0)} \right\}. \tag{36}$$

After similar transformations Eq. (27) can be written in the following form:

$$E_n(\mathbf{k}) = \frac{1}{\sqrt{2 - \gamma_{\mathbf{k}}^2}} \left\{ [a_+ + (-1)^n a_- \gamma_{\mathbf{k}}]^2 - J^2(\mathbf{k}) + \right.$$

$$\left. + [1 - \gamma_{\mathbf{k}}^2](J^2(0)\eta^2 - a_+^2) \right\}^{1/2}. \tag{37}$$

The comparison of the proposed dispersion equations can be readily done in the form of Eqs. (35) and (37). As seen, at $\mathbf{k} = 0$ ($\gamma_{\mathbf{k}} = 1$) they coincide. At small wave vectors the dispersion curves given by these equations agree very closely but the difference becomes more and more essential with rising wave vectors. If we use these equations to fit the experimental data to the calculated values we have that the magnetic properties, which, such as magnetic heat capacity, sample the whole Brillouin zone, can be described far better with the dispersion equation (27) [49,50] than with other dispersion equations proposed in literature.

Dispersion curves for the dispersion equation (27) (or (37)) are given in Fig. 16. As can be seen, the magnon spectrum is strongly anisotropic. For the directions in the basal *ab* plane the spectrum is characterized by more significant dispersion than for magnons with the wave vector normal to the basal plane.

For magnons with $\mathbf{k}$ in the basal plane the maximal frequency is

$$E_{\max} \approx J(0)\eta/\sqrt{2}. \tag{38}$$

The first estimate of the magnitude of the exchange field was obtained by Wachtel and Wheeler [18,24]. They used the Hamiltonian (20) and calculated the magnon spectrum of α-O_2 within a model with isotropic exchange interaction neglecting the intrasublattice coupling constant J_2 and assuming that the nearest neighbor number $z = n_1 + n_3 = 8$, $J_1 = J_3 \equiv J$ ($\alpha = 1$, $\kappa = 0$). To determine three unknown parameters J, A, and B they set two calculated center zone magnon frequencies to the experimental AFMR frequencies, obtaining two of three necessary equations. The third equation was derived by assuming that the magnon frequency at the zone edge is equal to 37.5 cm^{-1}, characteristic frequency obtained by Eremenko group [19–21]

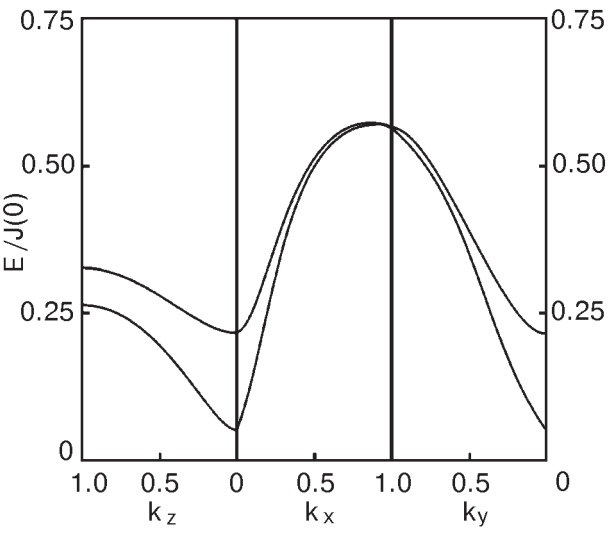

Fig. 16. Dispersion curves for magnon modes in α-O_2 .

from the sideband spectra in the double excitation bands $2^3\Sigma_g^- \to 2^1\Delta_g$ and $2^3\Sigma_g^- \to 2^1\Sigma_g^+$ (see Sec. 2). As a result, they obtained $J(0) = 32$ cm^{-1}.

But as were shown in Refs. 1 and 7, the model with isotropic exchange interaction by Wachtel and Wheeler is in contradiction with the low-temperature specific heat data. Namely, the analysis of the low-temperature specific heat of α-O_2 performed in Refs. 1 and 7 revealed that for $T < 10$ K, when the contribution of molecular librations is negligible, the sum of the lattice and magnon components to the specific heat with the latter calculated with the magnon spectrum from Refs. 18, 24 exceeds the experimental data significantly. Moreover, as was pointed out by Slusarev et al. [49,50], the magnetic susceptibility of α-oxygen, corresponding to the magnetic parameters found by Wachtel and Wheeler, exceeds the experimental susceptibility by a factor of 6.

The authors of Refs. 1 and 7 came up the opinion that the main drawback of Wachtel–Wheeler's approach was the assumption that the exchange interaction is isotropic and put forward the model that α-O_2 is a quasi-two-dimensional antiferromagnet, i.e., $\alpha << 1$. This conjecture launched a long discussion in literature [45,55–57] but subsequently obtained a direct support in an *ab initio* calculations of the exchange interaction of oxygen molecules [58,59].

Theory of magnetic properties (the magnetic heat capacity, the magnetic susceptibility, and the frequencies of antiferromagnetic resonance) of the two low-temperature phases as a quasi-2D Heisenberg system was developed by Slusarev et al. [49,50]. In order to obtain information on the parameters of the magnetic system of solid oxygen, the experimental magnetic heat capacity must be compared with theoretical estimations. The theoretical magnetic heat capacity is determined by the spin-wave spectrum $E(\mathbf{k})$ and can be written as a sum over two branches of the spectrum $E_1(\mathbf{k})$ and $E_2(\mathbf{k})$:

$$C_{\text{mag}}/R = \sum_{n=1,2} \frac{1}{(2\pi)^3} \int_{-\pi}^{\pi} d^3k \frac{(E_n/T)^2 \exp(E_n/T)}{[\exp(E_n/T) - 1]^2}. \quad (39)$$

The experimental points were obtained as a difference between the heat capacity C_V^{exp} and the phonon contribution. The former value was obtained from the data on C_P [60] and the $C_P - C_V$ correction, which was calculated using the data on the isothermal compressibility [42,61], and on the thermal expansion [1,7]. The phonon contribution was calculated [62] in the Debye approximation with $\Theta_D = 104$ K taking into account the $\Theta_D(T)$ dependence obtained from the temperature dependence of sound velocities [42,61,63]. The libron contribution is negligible in the given temperature range.

Thus, the magnon heat capacity Eq. (39) contains three variable parameters, and it is most convenient to use in this capacity the exchange field $J(0)$ and two dimensionless parameters α and κ. Sensitivity of the magnetic heat capacity to changes in these parameters can be readily seen from the low-temperature asymptotic for C_{mag}:

$$C_{\text{mag}}/R = \frac{4}{(2\pi)^{3/2}} \frac{(1 + \alpha - k/2)^{3/2}}{\sqrt{\alpha}\ \sqrt{1 + \alpha - 2k}} \times$$

$$\times \left(\frac{E_1(0)}{J(0)\eta}\right)^3 \left(\frac{E_1(0)}{T}\right)^{1/2} e^{-E_1(0)/T}. \quad (40)$$

As can be seen, the dimensionless interplane exchange coupling constant α enters into Eq. (40) as a singular factor, and thus the low-temperature magnon heat capacity is very sensitive to this parameter. The best choice obtained by comparison of the calculated and experimental magnetic heat capacity (see Fig. 17) is $J(0) = 125.9$ cm^{-1}; $\alpha = 0.025$. The fact that the inequality $\alpha << 1$ holds means that α-O_2 is a quasi-two-dimensional antiferromagnet.

The dimensionless intrasublattice exchange parameter κ also enters into Eq. (40) as a singular factor. For the quasi-two-dimensional antiferromagnet ($\alpha << 1$) it imposes on the magnitude of κ the condition

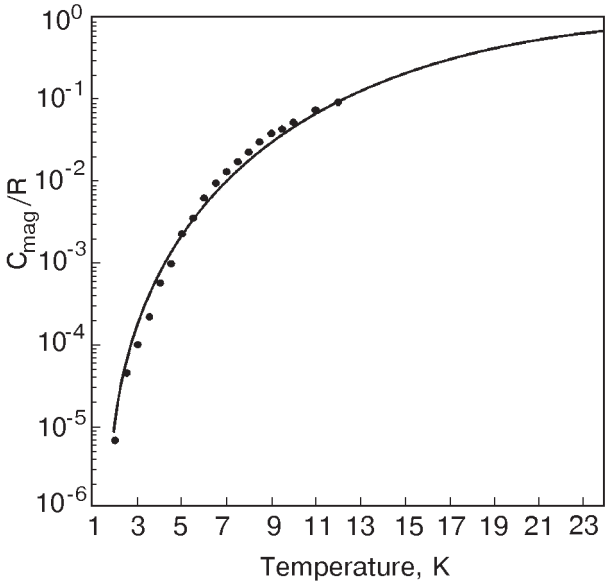

Fig. 17. Magnetic heat capacity. Experimental points — see text, solid curve is the best fit to Eq. (39).

$$\kappa < 1/2, \qquad (41)$$

which is a direct consequence of the condition of stability of the collinear antiferromagnet structure [64]. If the condition Eq. (41) is violated, the calculated magnon frequencies become imaginery for a region of wave vectors along the direction $\mathbf{k} = (0, k, 0)$. For the 3D antiferromagnet ($\alpha = 1$) the magnitude of κ instead the condition Eq. (41) should meet the condition

$$\kappa < 1. \qquad (42)$$

For the value of the exchange field obtained by the fit to the experimental data for the magnon thermal capacity ($J(0) = 125.9$ cm^{-1}), the maximum magnon frequency (see Fig. 16) $E_{\max} = 72.7$ cm^{-1}. The magnon frequencies at the Brillouin-zone boundaries for the magnons with the wave vector $\mathbf{k}$ in the *ab* plane are close to $E_{\max}$ (around 70 cm^{-1} for the both branches). For the magnons with $\mathbf{k}$ normal to the basal plane due to the anisotropy of the exchange interaction there is a gap between the two spectral branches at the boundary of the Brillouin zone. The edge frequencies for the two branches are

$$E_{\frac{1}{2}}(0,0,\pi) = \left[E_{\frac{1}{2}}^2(0) + \frac{4\alpha}{1-\kappa/2} J^2(0)\eta^2 \right]^{1/2}. \qquad (43)$$

For the adopted parameters we have the following estimates: $E_1(0,0,\pi) \approx 33.2$ cm^{-1}, $E_2(0,0,\pi) \approx \approx 42.4$ cm^{-1}, and the gap $\Delta_1 = E_2(0,0,\pi) - E_1(0,0,\pi)$ amounts to 9.2 cm^{-1}.

These theoretical estimates for the edge frequencies are very close to those obtained by Eremenko et al. [20,21] (38 and 75 cm^{-1}). It is important to stress that no spectroscopic data were used in their derivation and these estimates are based on the fit to the data on the magnon heat capacity and magnetic susceptibility.

It has been speculated [1], that the observed doubling of exciton-magnon absorption lines [65] is related to the discussed nature of the magnon spectrum of α-O_2 .

Allowance for the intrasublattice exchange interaction ($\kappa \neq 0$) makes magnons with wave vectors along *a* and *b* axes inequivalent. Degeneracy at the zone edge for the high-symmetry directions is lifted and another gap exists between the two spectral branches at the boundary of the Brillouin zone at $\mathbf{k} = (\pi,0,0)$ and $(0,\pi,0)$. The gap is proportional to the dimensionless intrasublattice coupling constant κ:

$$\Delta_2 = \frac{\kappa}{8\eta\sqrt{2}} \frac{E_2^2(0) - E_1^2(0)}{J(0)}. \qquad (44)$$

The gap is rather small but, in principle, measurable ($\Delta \approx 0.25$ cm^{-1}).

Recently, systematic Fourier transform infrared spectroscopy studies of electronic excitations in solid oxygen were carried out by Jodl group [32]. Though their data confirmed considerable anisotropy of the magnon spectrum, estimates for the magnon frequencies at the Brillouin-zone boundaries obtained in this study turned out to be significantly different from those obtained by Ere-

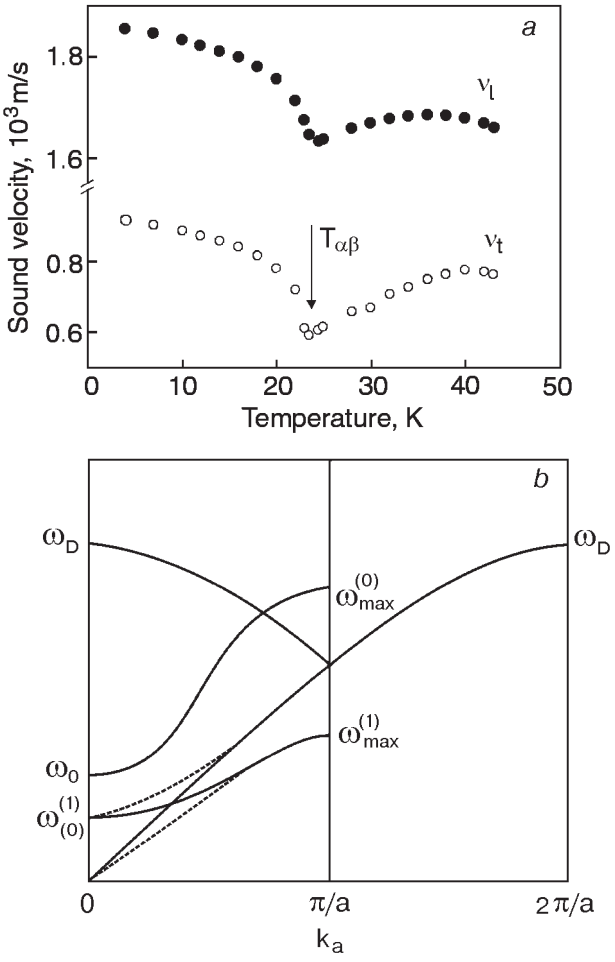

Fig. 18. Temperature dependence of the sound velocities in α- and β-O_2 [42,61] (*a*). Schematic dispersion curves of phonons and magnons in α-O_2 illustrating the way the phonon-magnon coupling results in strong temperature dependence of the phonon velocity. Solid curves are uncoupled acoustic translational (based upon crystallographic unit cell) and magnon modes (based upon magnetic unit cell), coupled modes in the folded zone are given by dashed curves. ω_0, $\omega^{(0)}_{\max}$ and $\omega^{(1)}_0$, $\omega^{(1)}_{\max}$ are respectively the zone center and zone edge magnon frequency at $T = 0$ K and at a nonzero temperature (*b*).

menko et al. [20,21]. This discrepancy needs clarification.

The dispersion equation (27) containes one important feature of dispersion curves which is lacking in other forms of the dispersion equation. Since the maximal energy of magnons described by Eq. (27) is proportional to the magnetic order parameter (Eq. (38)), which is a decreasing function of temperature, the dispersion curves of magnons are strongly temperature dependent. Among possible experimantal implications we note here the anomaly temperature dependence of the sound velocities [61,63].

A qualitative model which provides a possible explanation in which way the anomaly behavior of the sound velocities stems from the strong temperature dependence of the magnon dispersion curves is illustrated in Fig. 18. One can see, when the zone edge magnon frequency $\omega_{\max}^{(1)}$ decreases with temperature, the slope of the acoustic coupled phonon-magnon mode nearly goes to zero at the $\alpha-\beta$ transition.

Libron, magnon and phonon branches of the spectrum of elementary excitations exhibit essentially different anisotropy. The former two reveal significant anisotropy [1,7] while for the latter the anisotropy is far less pronounced [11]. Librons and magnons with the wave vectors in the *ab* plane is characterized by significant dispersion, while for librons and magnons propagating along the normal to the *ab* plane the band widths are comparatively small. The nonequivalence of the different spectral branches is due to the fact that the anisotropic and exchange interactions are more short-ranged than the isotropic interaction determining the phonon spectrum.

6. Summary

We have reviewed results on the lattice dynamics calculations concerning the elementary excitation spectra of α-, β-, and γ-oxygen. An important characteristic feature of solid oxygen as a magnetic system is an anomaly large coupling between lattice and magnetic subsystems. It was shown, in particular, that it is essential to include the Heisenberg term in the lattice dynamics calculations to explain the long-state problem of the anomalously large libron splitting in α-O_2. Developed an integrated scheme for lattice dynamics and spin-wave calculations provides a good approach for the theoretical treatment of the system. The calculated spectrum of magnons permits to describe the magnetic properties of α-O_2 in a fair agreement with experiment.

Among theoretical problems that remain to be solved are as follows:

– Detailed calculations of the dispersion curves and density of states for phonons, librons and magnons;

– Calculations of thermal and magnetic properties with obtained density of states;

– Calculations of anharmonic phonon and libron effects;

– Calculations of kinetic and relaxational properties;

– Lattice dynamics calculations of the high-pressure phases.

Acknoledgment

The authors dedicate this work to Prof. V. V. Eremenko on the occasion of his 70th birthday.

1. I. N. Krupskii, A. I. Prokhvatilov, Yu. A. Freiman, and A. I. Erenburg, *Fiz. Nizk. Temp.* **5**, 271 (1979) [*Sov. J. Low Temp. Phys.* **5**, 130 (1979)].
2. R. A. Alikhanov, *Zh. Eksp. Teor. Fiz.* **45**, 812 (1963) [*Sov. Phys. JETP* **18**, 556 (1964)].
3. R. A. Alikhanov, E. B. Vul, and Yu. G. Fedorov, *Acta. Cryst.* **A21,** 92 (1966).
4. R. A. Alikhanov, *JETP Lett.* **5**, 349 (1967).
5. M. F. Collins, *Proc. Phys. Soc*. **89**, 415 (1966) .
6. C. S. Barrett, L. Meyer, and J. Wasserman, *J. Chem. Phys.* **47**, 592 (1967) .
7. I. A. Burakhovich, I. N. Krupskii, A. I. Prokhvatilov, Yu. A. Freiman, and A. I. Erenburg, *JETP Lett*. **25,** 33 (1977) .
8. E. M. Hörl, *Acta Cryst*. **15**, 845 (1962) .
9. T. H. Jordan, W. E. Streib, H. W. Smith, and W. N. Lipscomb, *Acta. Cryst.* **17,** 777 (1964) .
10. Yu. A. Freiman and H. J. Jodl, to be published in *Phys. Rep.* (2002).
11. J. E. Jelinek, A. M. Karo, and L. J. Slutsky, *J. Phys. Chem. Solids* **33**, 1279; 1291 (1972) .
12. K. Kobashi, M. L. Klein, and V. Chandrasekharan, *J. Chem. Phys.* **71**, 843 (1979) .
13. A. P. Brodyanskii, V. A. Slusarev, and Yu. A. Freiman, *Fiz. Nizk. Temp.* **6**, 533 (1980) [*Sov. J. Low Temp. Phys*. **6**, 256 (1980)].
14. A. P. J. Jansen and A. van der Avoird, *J. Chem. Phys*. **86**, 3583; 3597 (1987) .
15. J. E. Cahill and G. E. Leroi, *J. Chem. Phys*. **51**, 97 (1969).
16. *Physics of cryocrystals,* V. G. Manzhelii and Yu. A. Freiman (eds.), NY, AIP Press (1997).
17. A. Helmy, K. Kobashi, and R. D. Etters *J. Chem. Phys.* **80**, 2782 (1984); Errata: **82**, 473 (1985).
18. E. J. Wachtel and R. G. Wheeler, *J. Appl. Phys.* **42**, 1581 (1971).
19. V. V. Eremenko, Yu. G. Litvinenko, and E. M. Ogneva, *Zh. Eksp. Theor. Fiz.* **48**, 1611 (1965).

20. V. V. Eremenko and Yu. G. Litvinenko, *Zh. Eksp. Theor. Phys*. **53**, 539 (1967) [*Sov. Phys. JETP* **26,** 350 (1968)].
21. Yu. G. Litvinenko, V. V. Eremenko, and T. I. Garber, *Phys. Status Solid* **30**, 49 (1968).
22. A. Landau, E. J. Allin, and H. L. Welsh, *Spectrochim. Acta* **18**, 1 (1962).
23. T. G. Blocker, M. A. Kinch, and F. G. West, *Phys. Rev. Lett.* **22**, 853 (1969).
24. E. J. Wachtel and R.G. Wheeler, *Phys. Rev. Lett*. **24**, 233 (1970) .
25. P. M. Mathai and E. J. Allin, *Can. J. Phys.* **49**, 1973 (1971).
26. E. G. Petrov, V. M. Loktev, and Yu. B. Gaididei, *Phys. Status Solid* **B41,** 117 (1970).
27. R. Bhandari and L. M. Falicov, *J. Phys. C: Solid State Phys*. **6**, 479 (1973).
28. T. Fujiwara, *J. Phys. Soc. Jpn.* **36**, 36 (1974).
29. Yu. B. Gaididei, V. M. Loktev, A. P. Prikhot'ko, and L. I. Shanskii, *Fiz. Nizk. Temp.* **1**, 1365 (1975) [*Sov. J. Low Temp. Phys.* **1**, 653 (1975)].
30. I. M. Pritula and L. V. Khashchina, *Fiz. Nizk. Temp.* **18**, 1035 (1992) [*Sov. J. Low Temp. Phys.* **18**, 727 (1992)].
31. S. Medvedev, *Elementarty Excitations in Solid Oxygen*, Thesis, University of Kaiserslautern (2002).
32. S. A. Medvedev, A. P. Brodyanski, and H. J. Jodl, *Phys. Rev.* **B63**, 184302 (2001).
33. M. Minenko, M. Vetter, A. Brodyanski, and H. J. Jodl, *Fiz. Nizk. Temp.* **26**, 947 (2000) [*Low Temp. Phys.* **26**, 699 (2000)].
34. R. D. Etters, K. Kobashi, and J. Belak, *Phys. Rev.* **B32**, 4097 (1985) .
35. D. Bier and H. J. Jodl, *J. Chem. Phys.* **81**, 1192 (1984).
36. A. F. Prikhot'ko, Yu. G. Pikus, L. I. Shanskii, and D. G. Danilov, *Sov. Phys. JETP* **42**, 253 (1985).
37. A. P. J. Jansen and A. van der Avoird, *Phys. Rev.* **B31**, 7500 (1985).
38. Yu. B. Gaididei, V. M. Loktev, and V. S. Ostrovskii, *Fiz. Nizk. Temp.* **11**, 740 (1985) [*Sov. J. Low Temp. Phys.* **11**, 406 (1985)].
39. Yu. B. Gaididei, V. M. Loktev, V. S. Ostrovskii, and A. P. Prikhot'ko, *Fiz. Nizk. Temp.* **12**, 61 (1986) [*Sov. J. Low Temp. Phys*. **12**, 36 (1986)].
40. B. Kuchta, *Chem. Phys*. **95**, 391 (1985).
41. M. L. Klein, D. Levesque, and J.-J. Weis, *Phys. Rev.* **B21**, 5785 (1980).
42. P. A. Bezugly, L. M. Tarasenko, and Yu. S. Ivanov, *Sov. Phys. Solid State* **10**, 1660 (1969).
43. H. Kiefte and M. J. Clouter, *J. Chem. Phys*. **62**, 4780 (1975).
44. R. J. Meier, J. H. Colpa, and H. Sigg, *J. Phys. C: Solid State Phys.* **17**, 4501 (1984).
45. R. J. Meier, *On the Magnetic and Optical Properties of Condensed Oxygen*, Thesis, Amsterdam University (1984).
46. *Kriokristally*, B. I. Verkin and A. F. Prikhot'ko (eds.), Naukova Dumka, Kiev (1983).
47. Yu. B. Gaididei and V. M. Loktev, *Sov. Phys. Solid State* **16**, 2226 (1975).
48. Yu. B. Gaididei and V. M. Loktev, *Ukr. Fiz. Zh.* **23**, 1147 (1978).
49. V. A. Slusarev, Yu. A. Freiman, and R. P. Yankelevich, *JETP Lett.* **30**, 270 (1979).
50. V. A. Slusarev, Yu. A. Freiman, and R. P. Yankelevich, *Fiz. Nizk. Temp.* **6**, 219 (1980) [*Sov. J. Low Temp. Phys.* **6**, 105 (1980)].
51. D. C. Mattis, *The Theory of Magnetism*, NY, Harper and Row publishers (1965).
52. F. Dyson, *Phys. Rev*. **102**, 1217; 1230 (1956).
53. S. V. Tyablikov, *Methods in the Quantum Theory of Magnetism,* Plenum, London (1967).
54. P. W. Anderson, *Phys. Rev*. **83**, 1260 (1951); **86**, 694 (1952) .
55. G. S. DeFotis, *Phys. Rev*. **B23**, 4714 (1981).
56. P. W. Stephens, R. J. Birgeneau, C. F. Majkrzak, and G. Shirane, *Phys. Rev.* **B28**, 452 (1983).
57. C. Uyeda, K. Sugiyama, and M. Date, *J. Phys. Soc. Jpn*. **54**, 1107 (1985).
58. M. C. van Hemert, P. E. S. Wormer, and A. van der Avoird, *Phys. Rev. Lett.* **51**, 1167 (1983).
59. P. E. S. Wormer and A. van der Avoird, *J. Chem Phys.* **81**,1929 (1984).
60. C. H. Fagerstroem and A. C. Hollis Hallett, *J. Low Temp. Phys.* **1**, 3 (1969).
61. P. A. Bezugly and L. M. Tarasenko, *Fiz. Nizk. Temp.* **1**, 1144 (1975) [*Sov. J. Low Temp. Phys*. **1**, 548 (1975).
62. A. I. Erenburg, *Structure, Thermal Expansion and Thermal Properties of Cryocrystals Formed by Linear Molecules.* Thesis, Institute for Low Temperature Physics and Engineering, Kharkov (1984).
63. B. I. Verkin, V. G. Manzhelii, and V. N. Grigor'ev, et al. *Handbook of Properties of Condensed Phases of Hydrogen and Oxygen*, Hemisphere Publishing Corporation NY (1991).
64. V. A. Slusarev, Yu. A. Freiman, and R. P. Yankelevich, *Fiz. Nizk. Temp.* **7**, 536 (1981) [*Sov. J. Low Temp. Phys*. **7**, 265 (1981)].
65. Y. B. Gaididei, V. M. Loktev, A. F. Prikhotko, and L. I. Shanskii, *Opt. Spectrosk. (USSR)* **41**, 855 (1975).